

Analysis of metabolic pathways and fluxes in a newly discovered thermophilic and ethanol-tolerant *Geobacillus* strain

Yinjie J. Tang^{1,8}, Rajat Sapra^{2,4}, Dominique Joyner^{1,3}, Terry C. Hazen^{1,3}, Samuel Myers⁵, David Reichmuth⁴, Harvey Blanch^{2,5,7}, and Jay D. Keasling^{1,2,5,6,7}

Running title: *flux analysis of an ethanol tolerant thermophile*

(1) Virtual Institute for Microbial Stress and Survival

(2) Joint Bio-Energy Institute, Emeryville, CA 94608

(3) Ecology Department, Lawrence Berkeley National Lab, Berkeley, 94720,

(4) Sandia National Laboratories, PO Box 969, Livermore, CA 94551-9951,

(5) Department of Chemical Engineering, University of California, Berkeley, CA 94720

(6) Department of Bioengineering, University of California, Berkeley, CA 94720

(7) Physical Biosciences Division, Lawrence Berkeley National Laboratory, Berkeley, CA 94720

(8) Department of Energy, Environmental and Chemical Engineering, Washington University, St Louis, MO63130

1 Abstract

2 A recently discovered thermophilic bacterium, *Geobacillus thermoglucosidasius*
3 M10EXG, ferments a range of C5 (e.g., xylose) and C6 sugars (e.g., glucose) and is tolerant to
4 high ethanol concentrations (10% v/v). We have investigated the central metabolism of this
5 bacterium using both *in vitro* enzyme assays and ¹³C-based flux analysis to provide insights into
6 the physiological properties of this extremophile and explore its metabolism for bioethanol or
7 other bioprocess applications. Our findings show that glucose metabolism in *G.*
8 *thermoglucosidasius* M10EXG proceeds via glycolysis, the pentose phosphate pathway, and the
9 TCA cycle; the Entner-Doudoroff pathway and transhydrogenase activity were not detected.
10 Anaplerotic reactions (including the glyoxylate shunt, pyruvate carboxylase and
11 phosphoenolpyruvate carboxykinase) were active, but fluxes through those pathways could not
12 be accurately determined using amino acid labelling. When growth conditions were switched
13 from aerobic to micro-aerobic conditions, fluxes (based on a normalized glucose uptake rate of
14 100 units (gm DCW)⁻¹·hr⁻¹) through the TCA cycle and oxidative pentose phosphate pathway
15 were reduced from 64±3 to 25±2 and from 30±2 to 19±2, respectively. The carbon flux under
16 microaerobic growth was directed to ethanol, L-lactate (>99% optical purity), acetate, and
17 formate. Under fully anaerobic conditions, *G. thermoglucosidasius* M10EXG used a mixed acid
18 fermentation process and exhibited a maximum ethanol yield of 0.38±0.07 mol mol⁻¹ glucose. *In*
19 *silico* flux balance modelling demonstrates that lactate and acetate production from *G.*
20 *thermoglucosidasius* M10EXG reduces the maximum ethanol yield by approximately three
21 folds, thus indicating that both pathways should be modified to maximize ethanol production.

22 **Key words:** C5 sugar, micro-aerobic, TCA cycle, anaplerotic pathway, flux balance model

1 Introduction

2 A recently discovered thermophilic ethanologen, *Geobacillus thermoglucosidasius*
3 M10EXG (M10EXG), is a facultative anaerobe that has an optimal growth temperature of 60°C
4 (Fong et al. 2006). It can ferment a range of C5 and C6 sugars and tolerate ethanol
5 concentrations of up to 10% (v/v) (Fong et al. 2006), which makes it an ideal microbe for
6 improved bio-ethanol production. Moreover, *Geobacillus* species have many other potential
7 industrial applications for production of various thermostable enzymes, exopolysaccharides and
8 bacteriocins; they have also been found to metabolize hydrocarbons in high temperature oil
9 fields (Nazina et al. 2005) as well as degrading herbicides (such as organophosphonates)
10 (McMullan et al. 2004). However, the genome sequence of this newly discovered *Geobacillus*
11 strain is not yet available, and as such there is no functional genomics data. In order to engineer
12 the metabolic pathways of the bacterium for optimizing ethanol production from C5 and C6
13 sugars, an understanding of the carbon fluxes and the maximum potential for ethanol production
14 is required. In this study, we used *in vitro* enzyme activity assays and a ¹³C-based isotopomer
15 flux model to investigate central metabolic pathways of this thermophilic organism as a function
16 of oxygen availability (Stephanopoulos et al. 1998; Tang et al. 2007a; Tang et al. 2007b;
17 Wiechert et al. 2001). To accomplish this, cells were grown in minimal medium containing
18 either [1-¹³C] or [2-¹³C]-labelled glucose as the sole carbon source, and the ¹³C-labeling patterns
19 of derivatized, intracellular amino acids were determined using gas chromatography-mass
20 spectrometry (GC-MS). An isotopomer model was then constructed to simulate all of the atom
21 transitions in the assumed biochemical network (based on both enzyme activity assay and
22 metabolic pathways of its closest sequenced species *G. kaustophilus* (Takami et al. 2004)) and
23 the label distribution in all central metabolites. We then searched for a set of active intracellular

1 metabolic pathways and flux distributions that predicted the inferred isotopomer distribution of
2 key metabolites resulting from the isotopomer pattern of the derivatized amino acids. We show
3 that in the absence of genome information our approach provides an effective way to map the
4 central pathways of a new fermentative organism (Tang et al. 2007e) and directly observe the
5 functional output (i.e., metabolic fluxes) of the transcriptome, proteome, and metabolic changes
6 under different growth conditions (Sauer 2004).

7

8 **Materials and Methods**

9 **Culture conditions.** M10EXG was obtained from the *Bacillus* Genetic Stock Center at
10 the Ohio State University (Cat # W9A44). A complete minimal medium was used (Fong et al.
11 2006) for the cell culture under defined conditions. Since singly labeled carbon substrate can
12 well resolve the Entner-Doudoroff pathway and pentose phosphate pathway, [1-¹³C] D-glucose
13 (10 g L⁻¹; >98%; Cambridge Isotope, Andover, MA) was used as the sole carbon source (Fischer
14 et al. 2004). For anaerobic or micro-aerobic experiments, the cultures were incubated in sealed
15 glass bottles with septum caps, and the headspace was filled with argon (anaerobic conditions) or
16 air (micro-aerobic conditions, air liquid volume ratio 1:1). For aerobic cell cultures, cells were
17 incubated in shake flasks at 200 rpm. All cultures with labeled medium were started with a ~3%
18 inoculation volume from cells that had been first grown in Tryptic Soy Broth (BD Biosciences,
19 San Jose, CA) to stationary phase and then sub-cultured into minimal medium with ~3%
20 inoculation volume to remove the effect of naturally labelled carbon sources from the initial
21 inocula. All cultures (aerobic, microaerobic, and anaerobic) were incubated at 60°C with
22 shaking at 200 rpm. Total biomass growth was monitored by measuring the optical density at a
23 wavelength of 600 nm (OD₆₀₀).

1 **Enzyme Assays.** Exponentially growing cells were centrifuged and the resulting cell
2 pellets were resuspended in 1 ml 100 mM Tris-HCl pH 7.4 and lysed by sonication for all
3 enzyme assays. Total protein concentration for cell lysates was determined using the Bradford
4 method (Bio-Rad, Hercules, CA) with bovine serum albumin as the standard. All chemicals and
5 coupling enzymes were purchased from Sigma Chemical (St. Louis, MO). All enzyme assays
6 were performed at 55°C and monitored spectroscopically at their respective wavelengths. All
7 enzyme assays were performed as previously reported (McKinlay et al. 2007; Sauer et al. 2004;
8 Terada et al. 1991; Van der Werf et al. 1997). In brief, an isocitrate lyase assay contained 25 mM
9 imidazole pH 6.8, 5 mM MgCl₂, 1 mM EDTA, 4 mM phenylhydrazine, and 1 mM D-L-
10 isocitrate; the absorbance at 324 nm was used to monitor forming osazone derivatives. The
11 oxaloacetate decarboxylase assay contained 41 mM triethanolamine-HCl (TEA) pH 8.0, 460 μM
12 MnCl₂, 300 μM β-NADH, 11 units mL⁻¹ of lactate dehydrogenase, and 2.3 mM oxaloacetate; the
13 absorbance at 340 nm was used to monitor β-NADH oxidation. The α-ketoglutarate
14 dehydrogenase assay contained 50 mM MOPS pH 7.4, 4 mM MgCl₂, 200 μM CaCl₂, 6 mM
15 thiamine pyrophosphate, 6.7 mM β-NAD⁺, 5.2 mM cysteine-HCl, and 25 mM α-ketoglutarate;
16 the absorbance at 340 nm was used to monitor the increase in β-NADH. The
17 phosphoenolpyruvate (PEP) carboxylase assay contained 100 mM Tris-acetate pH 8.5, 2 mM
18 potassium PEP, 10 mM KHCO₃, 10 mM magnesium acetate, and 1.17 M dioxane; the
19 absorbance at 340 nm was used to monitor β-NADH oxidation. The transhydrogenase assay
20 contained 50 mM Tris-HCl, pH 7.6, 2 mM MgCl₂, 500 μM β-NADH and 1 mM 3-acetylpyridine
21 adenine dinucleotide (APAD⁺); the absorbance at 375 nm was used to monitor the loss of
22 APAD⁺. The PEP carboxykinase assay contained 25 mM HEPES, pH 7.1, 50 mM KCl, 2 mM
23 MgCl₂, 50 mM NaHCO₃, 500 μM dithiothreitol, 20 μM β-NADH, 100 μM ADP-Mg, 5 mM

1 glucose, 4 units mL⁻¹ of malate dehydrogenase, 4 units mL⁻¹ of hexokinase and 1 mM PEP; the
2 absorbance at 340 nm was used to monitor β-NADH oxidation. The malic enzyme assay
3 contained 67 mM TEA pH 7.4, 3.5 mM malic acid, 333 μM NAD(P)⁺, and 5 mM MnCl₂; the
4 absorbance at 340 nm was used to monitor NAD(P)H oxidation. The pyruvate carboxylase assay
5 contained 95 mM TEA pH 8.0, 6.3 mM pyruvate, 0.11% BSA, 26 units mL⁻¹ malate
6 dehydrogenase, 50 μM acetyl CoA, 240 μM β-NADH, 15 mM KHCO₃, and 1 mM ATP; the
7 absorbance at 340 nm was used to monitor β-NADH oxidation. All activity calculations had the
8 basal reaction rate subtracts and were normalized for amount of protein added to the assay (Table
9 1).

10 **Analytical methods for metabolite concentrations, biomass composition, and**
11 **isotopomer labelling.** The concentrations of glucose, formate, lactate, acetate, succinate, and
12 ethanol in the medium were measured using enzyme linked assay kits (r-Biopharm, Darmstadt,
13 Germany). Biomass constituents (proteinogenic amino acid composition) were measured by the
14 Molecular Structure Center, University of California, Davis; the fatty acids of M10EXG were
15 measured by Microbial ID (Newark, DE) (Supplementary Table S1). Most fatty acids were
16 saturated in M10EXG (a fact that would lead to decreased membrane fluidity and allow cell
17 growth at high temperatures and high ethanol concentrations (Daron 1970; Sullivan et al. 1979)),
18 and the 16- and 17-carbon fatty acids (including branched-chain iso- and anteiso-) accounted for
19 ~80% of total fatty acids. The weight fractions of the various macromolecules were assumed to
20 be same as a typical bacterium: protein (52%), RNA (16%), DNA (3%), lipids (9%), and total
21 carbohydrate (17%) (Stephanopoulos et al. 1998). The biomass constitute information was used
22 to give the estimation of range for searching the optimal fluxes to biomass pools.

1 The GC-MS protocol for isotopomer measurement has been reported previously (Tang et
2 al. 2007d). In brief, protein in cell pellets (from 50 ml culture) was hydrolyzed in 6 M HCl at
3 100°C for 24 hours. The resulting amino acid mixture was derivatized in 100 μ L tetrahydrofuran
4 (THF) and 100 μ l N-(tert-butyldimethylsilyl)-N-methyl-trifluoroacetamide (Sigma-Aldrich, St.
5 Louis, MO) at 70°C for 1 hour and analyzed using a gas chromatograph (Model 6890, Agilent,
6 Wilmington, DE) equipped with a DB5 column and a mass spectrometer (Model 5973 Network,
7 Agilent, Wilmington, Delaware). Two types of positively charged species were used in the
8 model simulation: unfragmented amino acids, $[M-57]^+$, and fragmented amino acids that have
9 lost their α carboxyl group, $[M-159]^+$. The natural abundance of isotopes was corrected using a
10 published algorithm before using the data for calculating the label distribution (Hellerstein and
11 Neese 1999).

12 **Assumptions employed in isotopomer modelling.** The development of the isotopomer
13 model was based on six assumptions. (i) A quasi-steady state is assumed to be achieved using
14 batch culture as a convenient and less expensive approach (Sauer et al. 1999; Tang et al. 2007b).
15 This assumption is based on the fact that isotopic patterns of 14 proteinogenic amino acids did
16 not change (less than 1% difference) during the exponential growth phase (OD_{600} 0.4-0.9). (ii)
17 The central metabolic network in M10EXG was inferred from the pathways in closely-related
18 *Geobacillus kaustophilus* (only sequenced *Geobacillus* species) and *Bacillus subtilis*
19 (Christiansen et al. 2002; Sauer et al. 1997). (iii) The direction of flux was based on reaction
20 thermodynamics, as suggested by a previous flux study on *Bacillus subtilis* (Sauer et al. 1997);
21 considerations of potential reversibility of each reaction would make the model system highly
22 underdetermined (Zhao and Shimizu 2003), thus only reactions between PEP and oxaloacetate
23 were assumed reversible. (iv) Amino acids provide isotopomer information unique to their

1 precursors in the central metabolic pathways. To avoid possible inaccuracies resulting from
2 alternative amino acid biosynthesis routes, seven amino acids were used to determine ^{13}C fluxes
3 in central metabolism (Supplementary Table S2). These corresponding metabolites and their
4 amino acid precursors were pyruvate (alanine), acetyl-CoA (leucine), oxaloacetate (aspartic
5 acid), 2-oxo-glutarate (glutamate), phosphoenolpyruvate & erythrose-4-phosphate
6 (phenylalanine), and 3-phosphoglycerate (serine and glycine) (Sauer et al. 1997). (v) The
7 pathways included in the model were the tricarboxylic acid (TCA) cycle, pentose phosphate (PP)
8 pathway, the Entner-Doudoroff pathway, and anaplerotic reactions. Oxalacetate decarboxylase
9 and malic enzyme were not included in the model because of no activity was observed from *in*
10 *vitro* enzyme assays (Table 1). (vi) The fluxes $\text{PEP} \leftarrow \rightarrow \text{OAA}$ and $\text{Pyr} \leftarrow \rightarrow \text{OAA}$ could not be
11 clearly distinguished via isotopomer labelling; therefore, PEP and pyruvate were treated as a
12 single metabolite pool and the reactions between PEP/Pyr pool and OAA were assumed
13 reversible.

14 **Algorithm for ^{13}C based flux calculation.** The extra-cellular fluxes (production of
15 formate, lactate, acetate and ethanol) were measured directly, and fluxes to biomass pools were
16 calculated based on the biomass composition (Supplementary Table S1). These fluxes were used
17 as inputs to the isotopomer model and tightly constrained within measurement noise. The
18 remaining unknown fluxes were determined from isotopomer fractions, to identify the operative
19 intracellular metabolic reactions as described before (Tang et al. 2007b). In brief, the complete
20 fluxes were solved using the reaction stoichiometry and atom / isotopomer mapping matrices in
21 an iterative scheme to obtain the steady-state isotopomer distributions in the intracellular
22 metabolites pools. **To avoid getting trapped in a local minimum, the model applied a grid search**
23 **strategy (Antoniewicz et al. 2006):** with the glucose uptake rate under three oxygen conditions

1 normalized to a value of 100 units (gm DCW)⁻¹ hr⁻¹, the model exhaustively searched all
2 combinations of independent variables (metabolite fluxes). Since the pyruvate shunt reaction
3 (pyruvate+CO₂→oxaloacetate via pyruvate carboxylase) consumes CO₂ from the medium, the
4 fraction of ¹³CO₂ in the medium was also estimated. The step size of the grid search algorithm
5 was 1 (normalized to the glucose uptake rate of 100 units (gm DCW)⁻¹hr⁻¹) for unknown fluxes
6 and 0.01 for the ¹³CO₂ fraction. All possible flux combinations were searched to determine the
7 global minima of the objective function (Tang et al. 2007b):

$$\epsilon(v_n) = \sum_{i=1}^a \left(\frac{M_i - N_i(v_n)}{\delta_i} \right)^2$$

8
9 where v_n are the unknown fluxes to be optimized in the program, M_i are the measured MS data,
10 N_i are the corresponding model-simulated MS data, and δ_i are the corresponding standard
11 deviations in the GC-MS data (1~2%). The unknown metabolic fluxes were calculated to
12 minimize ϵ . To estimate the confidence interval for calculated fluxes, a Monte Carlo approach
13 was employed (Zhao and Shimizu 2003). In brief, 20 isotopomer concentration data sets were
14 generated by addition of normally distributed measurement noise to actual measurement data.
15 The same optimization routine was used to estimate the best-fit flux distribution from these data
16 sets. Confidence limits for each flux value were obtained from the probability distribution of
17 calculated flux resulting from the simulated data sets. The model program was developed using
18 MATLAB 7.0 (The Mathworks, Natick, MA). The calculations were carried out using a Quad-
19 Process Server (Finetec, San Jose, CA) at the Lawrence Berkeley National Laboratory.

20 ***In silico* flux balance analysis (FBA).** FBA was used to estimate ethanol production
21 potential by M10EXG and prioritize the pathways for genetic engineering. Since the genome
22 sequence and functional metabolic pathway information of M10EXG were not available, *in*
23 *silico* modelling was constructed using the Simpheny platform (Genomatica, San Diego, CA) to

1 coarsely predict the M10EXG metabolic network (Mahadevan et al. 2006), with the following
2 modifications: 1) two unique reactions found in *Geobacillus* strains (L-lactate dehydrogenase
3 and pyruvate carboxylase) were added to the model; 2) The biomass composition for the
4 M10EXG model is given in Supplementary Table S1. The model included ~1075 reactions and
5 ~760 constraints, and the flux calculation algorithm relied on implementing a series of
6 physicochemical constraints, including thermodynamic directionality, enzymatic capacity
7 constraints, and reaction stoichiometry constraints (Edwards and Palsson 2000a). Since the
8 number of reactions is much greater than the number of metabolites, the system requires the
9 assumption of an objective function for the *in silico* flux balance analysis, i.e, maximizing cell
10 growth or ethanol production (Stephanopoulos et al. 1998).

11 Results and Discussion

12 **Growth kinetics and cellular metabolites under various oxygen conditions.** Since
13 *Geobacillus thermoglucosidasius* M10EXG grows in a minimal glucose medium between 55-
14 65°C (its optimal growth temperature is 60°C) with glucose as the sole carbon source, the
15 bacterium contains complete biosynthesis pathways for all amino acids and other essential
16 metabolites. The average doubling time in the exponential phase in minimal glucose medium
17 was two hours under aerobic growth conditions and 3.5 hours under micro-aerobic conditions
18 (Figure 1), i.e., the doubling time at high temperature was not faster than that of mesophilic
19 bacteria (such as *E. coli*) under similar batch conditions (Shaikh et al. 2008). Under aerobic
20 conditions, M10EXG produced ~0.64 mol acetate mol glucose⁻¹ (Table 2). Acetate accumulation
21 in the medium can inhibit cell growth, especially for mesophilic bacteria (Lynd 1989), due to
22 change in the intracellular pH or inhibition of activities of key enzymes in central metabolism
23 (Luli and Strohl 1990; Tang et al. 2007c). The production of acetate by aerobically growing

1 bacteria is often observed when the carbon source is in excess, so bacteria can regulate acetyl-
2 CoA consumption rate and quickly generate ATP when the activity of key TCA cycle enzymes
3 (e.g., citrate synthase) are inhibited (Majewski and Domach 1990). Under microaerobic or
4 anaerobic conditions, the cells secreted lactate, ethanol, and formate, in addition to acetate (Table
5 2). Under completely anaerobic conditions, the L-lactate (>99% optical purity) production
6 increased to 0.89 mol L-lactate mol⁻¹ glucose, and the formate yield was ~1 mol mol⁻¹ glucose
7 (i.e., pyruvate-formate lyase replaced pyruvate dehydrogenase for acetyl-CoA production), while
8 the molar yield of ethanol was ~ 0.38 mol mol⁻¹ glucose. The large amounts of acids produced
9 reduced the pH in the medium from 7.6 to ~5, and the cells entered the death phase (lysed) under
10 micro-aerobic condition after 20 hrs (i.e., the OD₆₀₀ dropped after 20 hrs). Finally, M10EXG can
11 also grow in xylose minimal medium and exhibits similar growth kinetics under different oxygen
12 conditions (Supplementary Table S3), which makes this microorganism an ideal candidate for
13 bio-ethanol production from lignocellulosic biomass (contain up to 40% C5 sugars). However,
14 M10EXG mainly utilized glucose as carbon source when both glucose (C6) and xylose (C5)
15 were available (ratio 1:1) (Supplementary Table S4). This result indicates that the presence of
16 glucose may strongly inhibit xylose metabolism.

17 **¹³C-based flux analysis of intra-cellular pathways under aerobic and micro-aerobic**
18 **conditions.** Isotopomer flux models were developed based on assumed central metabolic
19 pathways to optimally fit all isotopomer data. The optimal flux distributions (based on a
20 normalized glucose uptake rate of 100 units (gm DCW)⁻¹ hr⁻¹) and the confidence intervals of
21 seven key intracellular fluxes (including glycolysis, PP pathway, TCA cycle and anapleurotic
22 pathways) under both aerobic and micro-aerobic conditions are shown in Figure 2. The flux
23 distribution results indicate that oxygen concentrations strongly affected the metabolic fluxes

1 through the central pathways. Under aerobic conditions, approximately two-thirds of the glucose
2 flowed through glycolysis (relative flux = 69) and the remainder through the pentose phosphate
3 pathway (flux = 30), while the flux through citrate synthase (into the TCA cycle) was 64. Under
4 micro-aerobic conditions, growth was slower (0.20 hr^{-1}) (Table 2), and the fluxes through TCA
5 cycle and PP pathway (G6P \rightarrow 6PG) were reduced to 25 and 19, respectively. *In vitro* assays
6 showed no evidence for transhydrogenase activity under our experimental conditions (Table 1).
7 Flux through the PP pathway was sensitive to growth rate, most likely because NADPH to
8 support biomass synthesis is mainly from PP pathway (Christiansen et al. 2002). On the other
9 hand, *B. subtilis* showed much higher PP pathway flux (~ 70) that varied less with specific
10 growth rate (Sauer et al. 1997). This is because *B. subtilis* can convert excess NADPH from the
11 PP pathway to NADH via the transhydrogenase reaction and as such has greater flexibility in
12 balancing redox (Dauner et al. 2001; Sauer et al. 1997).

13 The flux results indicate that there is no Entner-Doudneroff (ED) pathway activity under
14 either experimental condition, which is consistent with the lack of a phosphogluconate
15 dehydratase (a key ED pathway enzyme) in the annotated *Geobacillus kaustophilus* genome
16 (Alm et al. 2005) and with the fact that *Bacillus* species do not use the ED pathway (Goldman
17 and Blumenthal 1963). Several anapleurotic reactions in M10EXG (as inferred from the
18 *Geobacillus kaustophilus* genome annotation) were present based on *in vitro* enzyme assays
19 (Table 1): Pyruvate \rightarrow OAA (pyruvate shunt via pyruvate carboxylase), OAA \rightarrow PEP (via PEP
20 carboxykinase), and PEP \rightarrow OAA (via PEP carboxylase). The flux results indicate that these
21 anapleurotic reactions were down-regulated under micro-aerobic conditions: the OAA \rightarrow PEP /
22 Pyruvate flux declined from 54 to 37, and the combined flux from PEP and pyruvate to OAA
23 declined from 44 to 24. Those non-biomass-related anapleurotic reactions may provide M10EXG

1 central metabolism with flexibility to cope with various growth conditions (Tang et al. 2007b).
2 The glyoxylate shunt, which reduces carbon flow through the oxidative branch of the TCA cycle
3 (coupled with other anapleurotic pathways) and provides an alternative route for acetyl-CoA
4 metabolism, was also measurable under aerobic and micro-aerobic conditions in M10EXG
5 (Fischer and Sauer 2003).

6 **Analysis of anaerobic pathways of M10EXG.** Under anaerobic conditions, M10EXG
7 disposed part of the glucose through lactic acid and formic acid production. The formic acid
8 yield ($\sim 1 \text{ mol mole}^{-1}$ of glucose consumed) was approximately equal to the sum of the acetate
9 and ethanol yields, indicating that acetyl-CoA is a precursor to ethanol (via alcohol
10 dehydrogenase) and acetate under mixed acid fermentation (Figure 3). Based on the metabolite
11 measurements and the reported mixed acid fermentation pathway of *B. subtilis* (Cruz Ramos et
12 al. 2000), a simplified anaerobic pathway is proposed (Figure 3). Under anaerobic conditions,
13 carbon flux between glycolysis and the PP pathway can be directly calculated based on the
14 labelling information, because the flux ratio between the two pathways is reflected in the
15 labelling pattern of 3-phosphoglycerate (inferred from serine) and pyruvate (inferred from
16 alanine) (Sauer et al. 1997). Meanwhile, the *in vitro* activity of α -ketoglutarate dehydrogenase
17 was one order magnitude lower than that measured when oxygen was available (Table 1). The
18 data showed that the enzymes of the TCA cycle were significantly repressed under anaerobic
19 conditions (Table 1) and that the TCA cycle was mainly used for biosynthesis. The major carbon
20 fluxes were directed towards mixed acids and ethanol production, which could be directly
21 measured. Eight key fluxes were shown in Figure 3: the flux was through glucose-6-phosphate
22 dehydrogenase (entrance to the oxidative branch of the PP pathway) under anaerobic conditions
23 (flux=15); pyruvate was converted to lactate via L-lactate dehydrogenase (flux=89) or to acetyl-

1 CoA and formic acid via pyruvate formate lyase (flux=103); acetyl-CoA was mainly used for
2 ethanol (flux=38) and acetate (flux=61) production. Compared to micro-aerobic conditions,
3 formic acid production was eight-fold higher under anaerobic conditions, suggesting that
4 pyruvate formate-lyase (PFL) was induced under anaerobic conditions (note: FNR, a
5 transcriptional regulator to mediate PFL gene (Sawers and Suppmann 1992) is annotated in
6 *Geobacillus kaustophilus*). Under anaerobic conditions, M10EXG generated NADH primarily
7 from glycolysis (glyceraldehyde-3-phosphate dehydrogenase) (flux = 190 ± 4) and consumed
8 NADH mainly for lactate, ethanol, and acetate production (flux = 165 ± 7).

9 **Verification of the isotopomer flux model.** The isotopomer-based flux analysis used
10 herein is based on the labelling pattern of [^{13}C]-amino acids to infer the [^{13}C] labelling pattern of
11 key metabolic intermediates. By tracing the path of ^{13}C from singly-labelled carbon substrate to
12 those metabolites in the pathway network, an isotopomer model can predict the carbon flux
13 distribution through central metabolism. To check the reliability of the flux analysis results, a
14 Monte Carlo method was used to calculate confidence intervals of key intracellular fluxes to
15 estimate uncertainty from measurement noise and experimental variation (as illustrated in
16 Materials and Method section). The obtained confidence intervals for seven key intracellular
17 pathways in Figure 2 **showed** that reaction $\text{G6P} \rightarrow \text{6PG}$ was best determined (confidence intervals
18 for both aerobic and anaerobic conditions are within ± 2), since 1- [^{13}C]-glucose **was** good for
19 differentiating the reactions of the PP pathway from glycolysis (Fischer et al. 2004). However,
20 fluxes of anapleurotic reactions between the pyruvate/PEP pool and OAA pool had the highest
21 errors; for example, the confidence interval of $\text{OAA} \rightarrow \text{PEP}$ flux under aerobic conditions was
22 ± 38 . This result indicated that the isotopomer data were not sufficient to constrain these two
23 fluxes accurately. To further validate the calculated intracellular flux distribution, [$2\text{-}^{13}\text{C}$]

1 glucose was used as the carbon source and the labeling of resulting key amino acids was used to
2 estimate the flux distribution under both aerobic and micro-aerobic conditions. The results from
3 [2-¹³C] glucose experiments were qualitatively consistent with the results from [1-¹³C] glucose
4 experiments (Supplementary Figure S1). Fluxes through reactions of the PP pathway,
5 glycolysis, and the TCA cycle (via citrate synthase) were very similar (difference <5). In
6 contrast, the measured fluxes for PEP carboxylase, pyruvate shunt, and the glyoxylate shunt from
7 the experiments using [2-¹³C] glucose had larger differences (up to 10) compared to the
8 measured fluxes from experiments using [1-¹³C] glucose. Errors in calculated fluxes may arise
9 from several sources: 1) the isotopomer information may be insufficient to constrain certain
10 anapleurotic reactions very accurately; 2) measurement uncertainty of extracellular metabolites
11 in batch cultures; 3) protein degradation and reincorporation of metabolites from catabolized
12 amino acids into metabolic intermediates.

13 ***In silico* analyses of metabolic network for ethanol production.** Since genetic
14 engineering of thermophilic bacteria is very difficult, it will, therefore, be beneficial to know
15 which reactions are the most important targets for genetic manipulation to improve ethanol
16 production. As such, an *in silico* flux balance analysis (FBA) was performed to coarsely predict
17 the optimal cellular metabolism for ethanol production via Simpheny Software from Genomatica
18 (San Diego, CA) (Mahadevan et al. 2006). The FBA model did not require isotopomer
19 information or detailed kinetic parameters for individual metabolic reactions (Edwards and
20 Palsson 2000a; Edwards and Palsson 2000b). Although these models are underdetermined and
21 may not reflect the actual metabolic flux distribution if typical objective function is assumed
22 without any additional constraints (e.g., maximum biomass production, Supplementary Figure
23 S2), they have proven to be a useful tool to provide important guidelines to explore the target

1 pathways for genetic engineering (Stephanopoulos et al. 1998). The theoretical maximum yields
2 of acetate, ethanol, lactate, formate, and biomass, as well as the theoretical maximum growth rate
3 (assuming an average carbon substrate uptake rate of 5 mM glucose (gm DCW)⁻¹ hr⁻¹), were
4 estimated using the Simpheny model. The predicted maximum yields of the metabolites and
5 biomass were much higher than the corresponding measured yields (Table 2). A plot of the
6 theoretical maximum ethanol production rate as the function of lactate and acetate production
7 rates for two growth rates (0.1 hr⁻¹ and 0.2 hr⁻¹), with or without formate production, indicates
8 that mixed acid production or a high growth rate significantly reduce the ethanol production rate
9 (Figure 4), because the mixed acid fermentation and biomass growth compete for the precursors
10 and reducing power (NADH) with ethanol production. Lactate production (by L-lactate
11 dehydrogenase) has the largest impact on ethanol yield followed by acetate production (acetate
12 kinase and phosphotransacetylase), while formate production (by pyruvate-formate lyase) has the
13 least impact on ethanol yield.

14 When growth rate maximization was used as the objective function, model results (Figure
15 5, the three dotted arrows linking the measured ethanol fluxes with the corresponding measured
16 growth rates) indicated that ethanol production by M10EXG was much lower than the theoretical
17 value. Meanwhile, the growth rate and all fluxes through reactions of the PP pathway and TCA
18 cycle declined when more ethanol production was specified (Figure 5). The TCA cycle and
19 oxidative PP pathway appeared to be the most sensitive to ethanol production, indicated by the
20 slopes of the fluxes through each pathway as a function of ethanol production. Those pathways
21 must be sufficiently down-regulated in order to produce high levels of ethanol. On the other
22 hand, the non-oxidative PP pathway (G3P+S7P→E4P+F6P via transaldolase) appeared to be
23 relatively insensitive to ethanol production.

1 Summary

2 The rising cost and use of fossil fuels has renewed focus on lignocellulosic ethanol (Lin
3 and Tanaka 2006) production via simultaneous saccharification and fermentation process (SSF)
4 (Lin and Tanaka 2006). However, enzymes employed to hydrolyze lignocellulosic biomass to
5 simpler sugars for fermentation generally have temperature optimum of around 55°C, whereas
6 the industrial organisms used to ferment the sugars to ethanol or other products (e.g.,
7 *Saccharomyces cerevisiae* (Antoni et al. 2007) and *E. coli* (Dien et al. 2003)) have a lower
8 operating temperature. Secondly, yeast cannot typically ferment C5 sugars (Sonderegger et al.
9 2004) such as xylose, a major component of lignocellulosic biomass. Furthermore, common
10 thermophilic ethanologens, e.g., *Clostridium thermosaccharolyticum*, are strict anaerobes (Lin
11 and Tanaka 2006) and cannot tolerate high ethanol concentrations (>4% w/v) (Fong et al. 2006).
12 *Geobacillus thermoglucosidasius* M10EXG overcomes some of these aforementioned limitations
13 and has many potential advantages for ethanol or other bio-product production: it tolerates high
14 ethanol concentrations (> 10% v/v); it can utilize a wide range of substrates (particularly
15 pentoses and insoluble substrates), which makes it an attractive organism for simultaneous
16 saccharification and fermentation of lignocellulosic biomass; there are lower risks of
17 contamination by other microorganisms (Akao et al. 2007) due to growth at high temperatures;
18 the growth medium will have desirable properties at high temperatures (reduced viscosity,
19 increased diffusion rates and substrate solubility, reduced energy requirements for mixing, and
20 the possibility of combining the fermentation and distillation processes to continuously extract
21 ethanol) (Lin and Tanaka 2006; Lynd 1989). This study investigates this species' metabolic
22 network via *in vitro* enzyme assays and ¹³C based flux analysis. The obtained information

1 provides guidelines for engineering the metabolic pathways for bioethanol production as well as
2 other environmental and industrial applications.

3 **Acknowledgements**

4 We thank Dr. Steve Van Dien (Genomatica) for helping with the Simpheny model and
5 Jeannie Chu for helping with metabolite measurement. Financial support for this research was
6 provided by the Sandia National Laboratories Laboratory Directed Research and Development
7 Program. Sandia is a multi-program laboratory operated by the Sandia Corporation, a Lockheed
8 Martin Company, for the United States Department of Energy under Contract DE-AC04-
9 94AL85000. D.J. and T.C. H. acknowledges support by the Virtual Institute for Microbial Stress
10 and Survival (<http://VIMSS.lbl.gov>) supported by the U.S. Department of Energy, Office of
11 Science, Office of Biological and Environmental Research, Genomics: GTL Program through
12 contract DE-AC02-05CH11231 between the Lawrence Berkeley National Laboratory and the US
13 Department of Energy. This work is also a part of the Joint BioEnergy Institute supported by the
14 U.S. Department of Energy.

15 **Financial Interest**

16 Jay D. Keasling has a consulting relationship with and a financial interest in Amyris and
17 a financial interest in LS9, two biofuel companies.

1 **References**

- 2 Akao S, Tsuno H, Cheon J. 2007. Semi-continuous L-lactate fermentation of garbage without
3 sterile condition and analysis of the microbial structure. *Water Research* 41:1774-1780.
- 4 Alm EJ, Huang KH, Price MN, Koche RP, Keller K, Dubchak IL, Arkin AP. 2005. The
5 MicrobesOnline Web site for comparative genomics. *Genome Res.* **15**:1015-1022.
- 6 Antoni D, Zverlov VV, Schwarz WH. 2007. Biofuels from microbes. *Appl Microbiol*
7 *Biotechnol.* 77(1):23-35.
- 8 Antoniewicz MR, Kelleher JK, Stephanopoulos G. 2006. Determination of confidence intervals
9 of metabolic fluxes estimated from stable isotope measurements. *Metabolic Engineering*
10 8(4):324-37.
- 11 Christiansen T, Christensen B, Nielsen J. 2002. Metabolic network analysis of *Bacillus clausii*
12 on minimal and semirich medium using ¹³C-Labeled glucose. *Metabolic*
13 *Engineering*(4):159-169.
- 14 Cruz Ramos H, Hoffmann T, Marino M, Nedjari H, Presecan-Siedel E, Dreesen O, Glaser P,
15 Jahn D. 2000. Fermentative Metabolism of *Bacillus subtilis*: Physiology and Regulation
16 of Gene Expression. *Journal of Bacteriology* 182(11):3072-80.
- 17 Daron HH. 1970. Fatty Acid Composition of Lipid Extracts of a Thermophilic *Bacillus* Species.
18 *Journal of Bacteriology* 101(1):145-151.
- 19 Dauner M, Bailey JE, Sauer U. 2001. Metabolic flux analysis with a comprehensive isotopomer
20 model in *Bacillus subtilis*. *Biotechnology and Bioengineering* 76(2):144-156.
- 21 Dien BS, Cotta MA, Jeffries TW. 2003. Bacteria engineered for fuel ethanol production: current
22 status. *Appl Microbiol Biotechnol.* 63(3):258-66.
- 23 Edwards JS, Palsson BO. 2000a. The *Escherichia coli* MG1655 *in silico* metabolic genotype: Its
24 definition, characteristics, and capabilities. *PNAS* 97(10):5528–5533.
- 25 Edwards JS, Palsson BO. 2000b. Robustness Analysis of the *Escherichia coli* Metabolic
26 Network. *Biotechnology Progress* 16:927-939.
- 27 Fischer E, Sauer U. 2003. A novel metabolic cycle catalyzes glucose oxidation and anaplerosis
28 in hungry *Escherichia coli*. *J Biol Chem.* 278(47):46446-51.
- 29 Fischer E, Zamboni N, Sauer U. 2004. High-throughput metabolic flux analysis based on gas
30 chromatography-mass spectrometry derived ¹³C constraints. *Analytical Biochemistry*
31 325:308-316.
- 32 Fong JC, Svenson CJ, Nakasugi K, Leong CT, Bowman JP, Chen B, Glenn DR, Neilan BA,
33 Rogers PL. 2006. Isolation and characterization of two novel ethanol-tolerant facultative-
34 anaerobic thermophilic bacteria strains from waste compost. *Extremophiles* 10(5):363-72.
- 35 Goldman M, Blumenthal HJ. 1963. Pathways of glucose catabolism in *Bacillus subtilis*. *Journal*
36 *of Bacteriology* 86:303-11.
- 37 Hellerstein MK, Neese RA. 1999. Mass isotopomer distribution analysis at eight years:
38 theoretical, analytic, and experimental considerations. *American Journal of Physiology-*
39 *Endocrinology and Metabolism* 276(6):E1146-E1170.
- 40 Lin Y, Tanaka S. 2006. Ethanol fermentation from biomass resources: current state and
41 prospects. *Applied Microbiology and Biotechnology* 69:627-642.
- 42 Luli GW, Strohl WR. 1990. Comparison of growth, acetate production, and acetate inhibition of
43 *Escherichia coli* strains in batch and fed-batch fermentations. *Applied and Environmental*
44 *Microbiology* 56(4):1004-1011.

- 1 Lynd LR. 1989. Production of Ethanol from Lignocellulosic Materials Using Thermophilic
2 Bacteria: Critical Evaluation of Potential and Review. Fiechter A, editor. Heidelberg:
3 Springer-Verlag. 1-52 p.
- 4 Mahadevan R, Bond DR, Butler JE, Esteve-Nunez A, Coppi MV, Palsson BO, Schilling CH,
5 Lovley DR. 2006. Characterization of metabolism in the Fe(III)-reducing organism
6 *Geobacter sulfurreducens* by constraint-based modeling. Applied and Environmental
7 Microbiology 72(2):1558-68.
- 8 Majewski RA, Domach MM. 1990. Simple Constrained-Optimization View of Acetate Overflow
9 in *E. coli*. Biotechnology and Bioengineering 35(7):732-38.
- 10 McKinlay JB, Shachar-Hill Y, Zeikus JG, Vieille C. 2007. Determining *Actinobacillus*
11 *succinogenes* metabolic pathways and fluxes by NMR and GC-MS analyses of ¹³C-
12 labeled metabolic product isotopomers. Metabolic Engineering 9(2):177-192.
- 13 McMullan G, Christie JM, Rahman TJ, Banat IM, Ternan NG, Marchant R. 2004. Habitat,
14 applications and genomics of the aerobic, thermophilic genus *Geobacillus*. Biochemical
15 Society Transactions 32(2):214-7.
- 16 Nazina TN, Sokolova DSh, Grigoryan AA, Shestakova NM, Mikhailova EM, Poltarau AB,
17 Tourova TP, Lysenko AM, Osipov GA, Belyaev SS. 2005. *Geobacillus jurassicus* sp.
18 nov., a new thermophilic bacterium isolated from a high-temperature petroleum reservoir,
19 and the validation of the *Geobacillus* species. Syst. Appl. Microbiol. 28(1):43-53.
- 20 Sauer U. 2004. High-throughput phenomics: experimental methods for mapping fluxomes.
21 Current Opinion in Biotechnology 15:58-63.
- 22 Sauer U, Canonaco F, Heri S, Perrenon A, Fischer E. 2004. The soluble and membrane-bound
23 transhydrogenases UdhA and PntAB have divergent functions in NADPH metabolism of
24 *Escherichia coli*. Journal of Biological Chemistry 279(8):6613-6619.
- 25 Sauer U, Hatzimanikatis V, Bailey JE, Hochuli M, Szyperski T, Wuthrich K. 1997. Metabolic
26 fluxes in riboflavin-producing *Bacillus subtilis*. Nature Biotechnology 15(5):448-52.
- 27 Sauer U, Lasko DR, Fiaux J, Hochuli M, Glaser R, Szyperski T, Wuthrich K, Bailey JE. 1999.
28 Metabolic flux ratio analysis of genetic and environmental modulations of *Escherichia*
29 *coli* central carbon metabolism. Journal of Bacteriology 181(21):6679-6688.
- 30 Sawers G, Suppmann B. 1992. Anaerobic Induction of Pyruvate Formate-Lyase Gene
31 Expression Is Mediated by the ArcA and FNR Proteins. Journal of Bacteriology
32 174(11):3474-3478.
- 33 Shaikh AS, Tang YJ, Mukhopadhyay A, Keasling JD. 2008. Isotopomer Distributions in Amino
34 Acids from a Highly Expressed Protein as a Proxy for Those from Total Protein. Anal
35 Chem. 80 (3):886-890.
- 36 Sonderegger M, Jeppsson M, Larsson C, Gorwa-Grauslund MF, Boles E, Olsson L, Spencer-
37 Martins I, Hahn-Hägerdal B, Sauer U. 2004. Fermentation performance of engineered
38 and evolved xylose-fermenting *Saccharomyces cerevisiae* strains. Biotechnol Bioeng.
39 87(1):90-8.
- 40 Stephanopoulos GN, Aristidou AA, Nielsen J. 1998. Metabolic Engineering Principles and
41 Methodologies. San Diego: Academic Press. 75, 120-130 p.
- 42 Sullivan KH, Hegeman GD, Cordes EH. 1979. Alteration of the Fatty Acid Composition of
43 *Escherichia coli* by Growth in the Presence of Normal Alcohols. Journal of Bacteriology
44 138(1):133-138.

- 1 Takami H, Takaki Y, Chee GJ, Nishi S, Shimamura S, Suzuki H, Matsui S, Uchiyama I. 2004.
2 Thermoadaptation trait revealed by the genome sequence of thermophilic *Geobacillus*
3 *kaustophilus*. *Nucleic Acids Res.* 32(21):6292-6303.
- 4 Tang YJ, Chakraborty R, Martin HG, Chu J, Hazen TC, Keasling JD. 2007a. Flux analysis of
5 central metabolic pathways in *Geobacter metallireducens* during reduction of soluble
6 Fe(III)-NTA. *Applied and Environmental Microbiology* 73(12):3859-3864.
- 7 Tang YJ, Hwang JS, Wemmer D, Keasling JD. 2007b. The *Shewanella oneidensis* MR-1
8 fluxome under various oxygen conditions. *Applied and Environmental Microbiology*
9 73(3):718-29.
- 10 Tang YJ, Meadows AL, Keasling JD. 2007c. A kinetic model describing *Shewanella oneidensis*
11 MR-1 growth, substrate consumption, and product secretion. *Biotechnology and*
12 *Bioengineering* 189(3):894-901.
- 13 Tang YJ, Meadows AL, Kirby J, Keasling JD. 2007d. Anaerobic central metabolic pathways in
14 *Shewanella oneidensis* MR-1 reinterpreted in the light of isotopic metabolite labeling.
15 *Journal of Bacteriology* 189(3):894-901.
- 16 Tang YJ, Pingitore F, Mukhopadhyay A, Phan R, Hazen TC, Keasling JD. 2007e. Pathway
17 confirmation and flux analysis of central metabolic pathways in *Desulfovibrio vulgaris*
18 Hildenborough using GC-MS and FT-ICR mass spectrometry. *Journal of Bacteriology*
19 189(3):940-949.
- 20 Terada K, Murata T, Izui K. 1991. Site-Directed Mutagenesis of Phosphoenolpyruvate
21 Carboxylase from *E. coli*: The Role of His⁵⁷⁹ in the Catalytic and Regulatory Functions.
22 *J. Biochem.* 109:49 - 54.
- 23 Van der Werf MJ, Guettler MV, Jain MK, Zeikus JG. 1997. Environmental and physiological
24 factors affecting the succinate product ratio during carbohydrate fermentation by
25 *Actinobacillus* sp. 130Z. *Arch Microbiol.* 167(6):332-342.
- 26 Wiechert W, Mollney M, Petersen S, de Graaf AA. 2001. A Universal Framework for ¹³C
27 Metabolic Flux Analysis. *Metabolic Engineering* 3:265-283.
- 28 Zhao J, Shimizu K. 2003. Metabolic flux analysis of *Escherichia coli* K12 grown on ¹³C-labeled
29 acetate and glucose using GC-MS and powerful flux calculation method. *Journal of*
30 *Biotechnology* 101:101-117.

31
32

1 Figure and Table Captions

2 **Figure 1:** Growth kinetics of M10EXG under three oxygen conditions: □ aerobic, ◇ micro-
3 aerobic, ○ anaerobic.

4

5 **Figure 2.** Pathways and flux distributions of glucose metabolism under aerobic (top) and micro-
6 aerobic (bottom) conditions. The amino acids used for isotopomer models were shown in
7 parentheses. The glucose uptake rates were normalized to a value of 100. Dotted lines indicate
8 that the pathways are not active. Abbreviations: Acetyl-CoA, acetyl-coenzyme A; CIT, citrate;
9 E4P, erythrose-4-phosphate; C1, 5,10-Me-THF; F6P, fructose-6-phosphate; G6P, glucose-6-
10 phosphate; 6PG, 6-phosphogluconate; ICT, isocitrate; MAL, malate; OAA, oxaloacetate; OXO,
11 2-oxoglutarate; PEP, phosphoenolpyruvate; PGA, 3-phosphoglycerate; C5P, ribose-5-phosphate
12 (or ribulose-5-phosphate or xylulose-5-phosphate); S7P, sedoheptulose-7-phosphate; SUC,
13 succinate; T3P, triose-3-phosphate.

14

15 **Figure 3.** M10EXG mixed acid fermentation. The abbreviations were the same as those in
16 Figure 2. Key reactions (and their corresponding relative fluxes): 1. glucose-6-phosphate
17 isomerase; 2. glucose-6-phosphate dehydrogenase; 3. T3P dehydrogenase; 4. L-lactate
18 dehydrogenase; 5. pyruvate-formate lyase; 6. acetaldehyde dehydrogenase; 7. alcohol
19 dehydrogenase; 8. phosphate acetyltransferase/acetate kinase. The arrows were drawn in
20 proportion to the fluxes. Fluxes below 10% of the glucose uptake rate were represented by non-
21 scaled hairlines.

22

1 **Figure 4.** Effect of mixed acids production and biomass growth rate on ethanol production as
2 calculated by the FBA model. The glucose uptake rate was set to 5 mmol hr⁻¹ g⁻¹ biomass. The
3 units for ethanol and acids production rates are mmol hr⁻¹ g⁻¹ biomass. (a) Growth rate = 0.1 hr⁻¹,
4 formate production = 0. (b) Growth rate = 0.2 hr⁻¹, formate production = 0. (c) Growth rate =
5 0.1 hr⁻¹, formate production was assumed to equal the sum of the ethanol and acetate production
6 rates; (d) Growth rate = 0.2 hr⁻¹, formate production was assumed to equal the sum of the ethanol
7 and acetate production rates.

8
9 **Figure 5.** Change in central metabolism as a function of ethanol production as predicted by the
10 *in silico* flux balance model (Simpheny). The objective function used for the calculations was the
11 maximal biomass production. Symbols: growth rate (○); flux into the TCA cycle via citrate
12 synthase (▲); flux into the pentose phosphate pathway via glucose 6-phosphate dehydrogenase
13 (◆) and via transaldolase (GAP+S7P→E4P+F6P) (●); flux through the pyruvate shunt (■). The
14 three dashed arrows **linked** the measured ethanol flux values with their corresponding measured
15 growth rates for the three growth conditions (aerobic, micro-aerobic, and anaerobic). The fact
16 that the lines (skewed dashed arrows) **were** not vertical indicates a difference between *in silico*
17 model predicted flux (optimal metabolism) and experimentally measured flux (actual
18 metabolism).

19
20 **Table 1.** Enzyme activities in cell extracts of *Geobacillus thermoglucosidasius* M10EXG under
21 three oxygen conditions (n=3).

22

1 **Table 2.** Growth kinetics and yields of ethanol and organic acids under the three oxygen
2 conditions: aerobic growth ($G + O_2$), micro-aerobic growth ($G + \mu O_2$), anaerobic growth ($G -$
3 O_2).

Figures

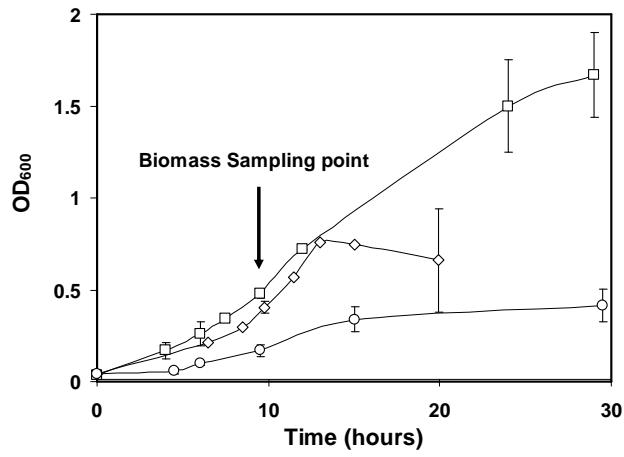


Figure 1. Growth kinetics of M10EXG under three oxygen conditions: □ aerobic, ◇ micro-aerobic, ○ anaerobic.

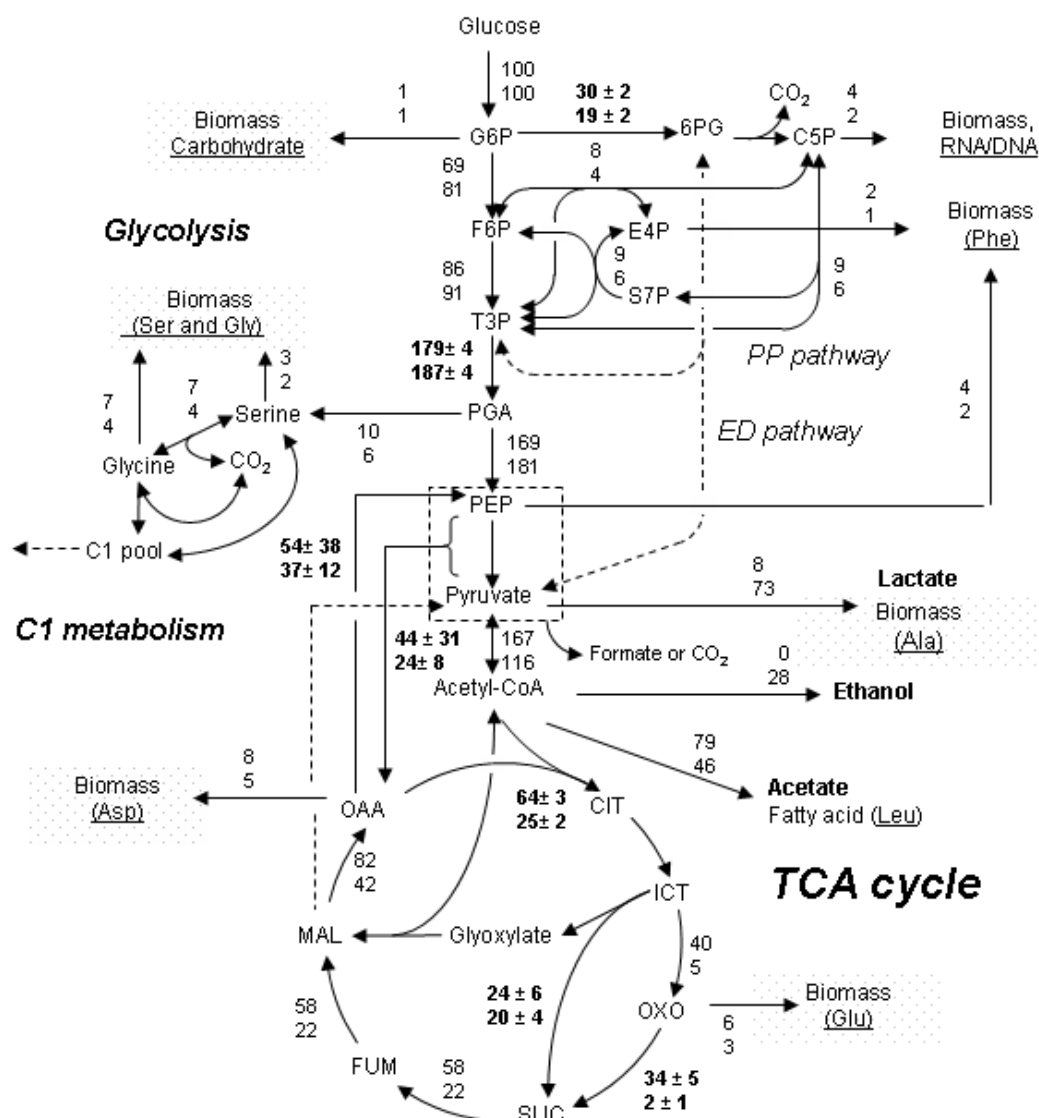


Figure 2. Pathways and flux distributions of glucose metabolism under aerobic (top) and microaerobic (bottom) conditions. The amino acids used for isotopomer models were shown in parentheses. The glucose uptake rates were normalized to a value of 100. **Dotted lines indicate that the pathways are not active.** Abbreviations: Acetyl-CoA, acetyl-coenzyme A; CIT, citrate; E4P, erythrose-4-phosphate; C1, 5,10-Me-THF; F6P, fructose-6-phosphate; G6P, glucose-6-phosphate; 6PG, 6-phosphogluconate; ICT, isocitrate; MAL, malate; OAA, oxaloacetate; OXO, 2-oxoglutarate; PEP, phosphoenolpyruvate; PGA, 3-phosphoglycerate; C5P, ribose-5-phosphate (or ribulose-5-phosphate or xylulose-5-phosphate); S7P, sedoheptulose-7-phosphate; SUC, succinate; T3P, triose-3-phosphate.

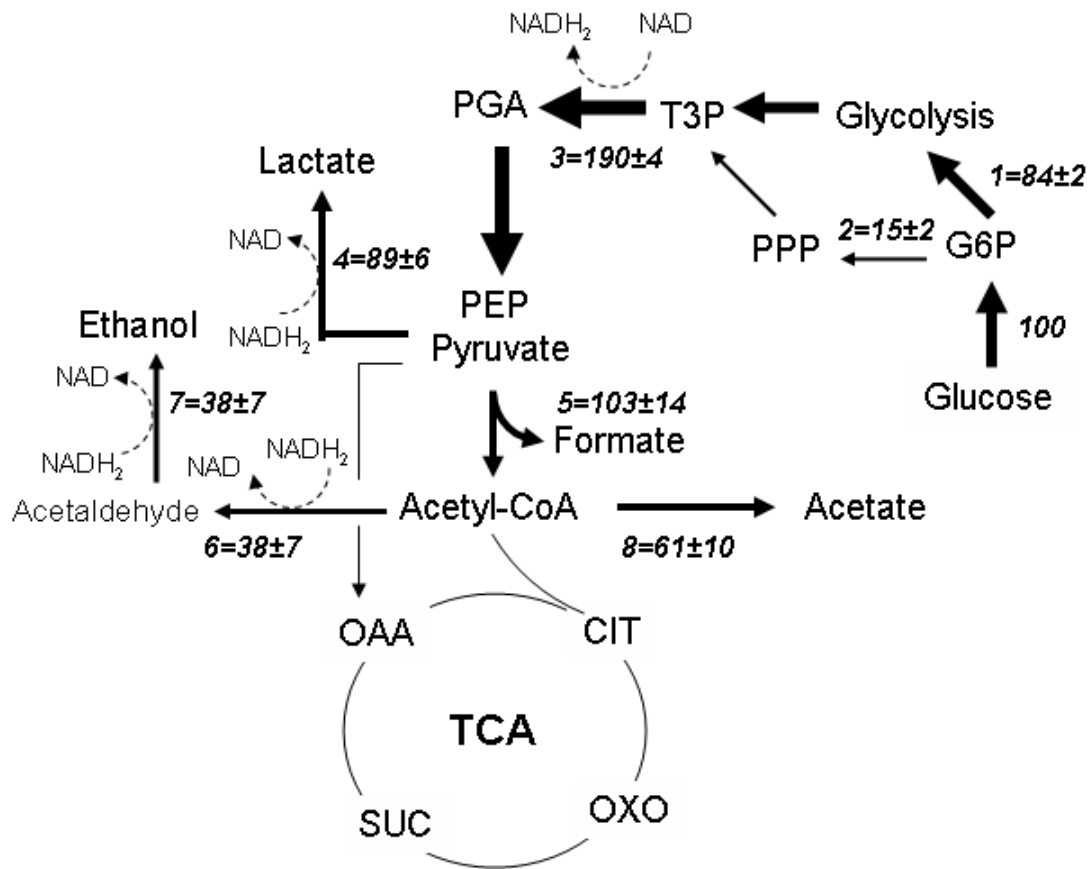


Figure 3. M10EXG mixed acid fermentation. The abbreviations were the same as those in Figure 2. Key reactions (and their corresponding relative fluxes): 1. glucose-6-phosphate isomerase; 2. glucose-6-phosphate dehydrogenase; 3. T3P dehydrogenase; 4. L-lactate dehydrogenase; 5. pyruvate-formate lyase; 6. acetaldehyde dehydrogenase; 7. alcohol dehydrogenase; 8. phosphate acetyltransferase/acetate kinase. The arrows were drawn in proportion to the fluxes. Fluxes below 10% of the glucose uptake rate were represented by non-scaled hairlines.

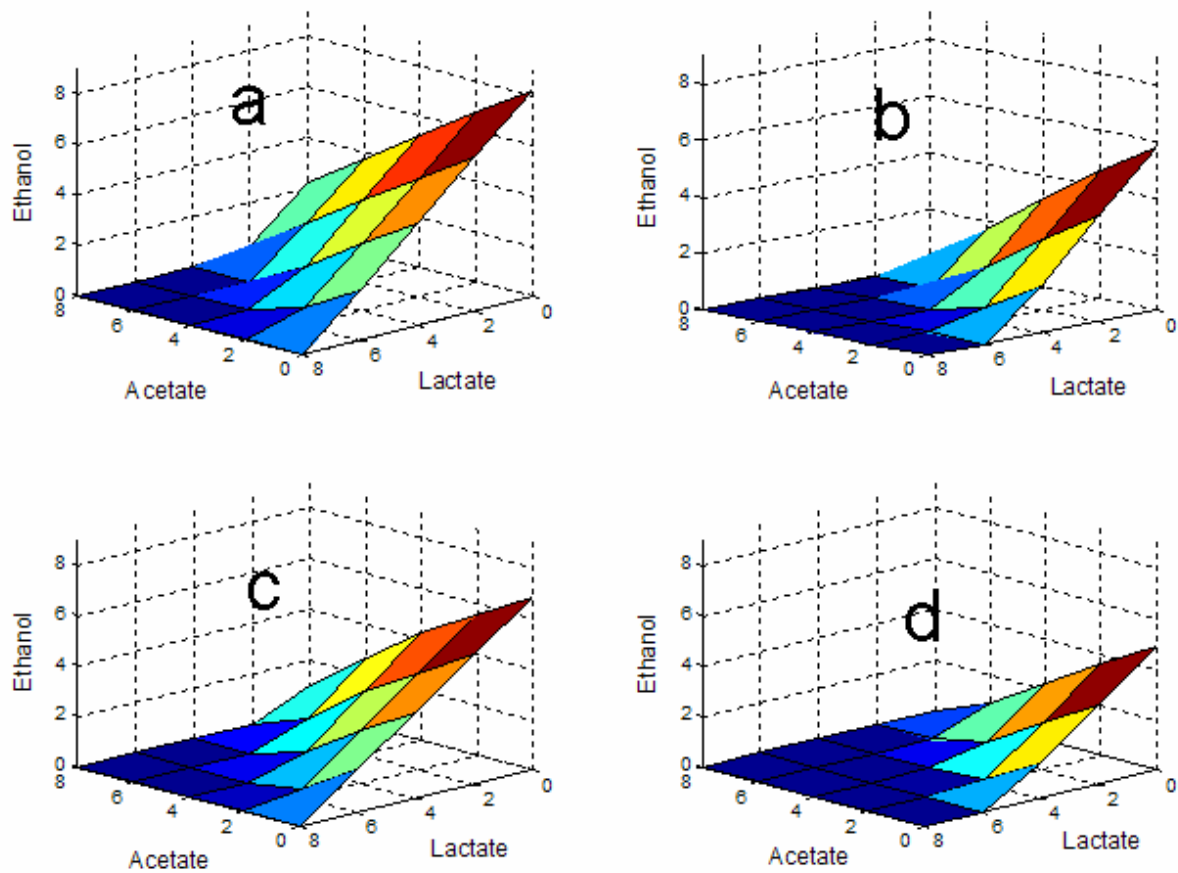


Figure 4. Effect of mixed acids production and biomass growth rate on ethanol production as calculated by the FBA model. The glucose uptake rate was set to $5 \text{ mmol hr}^{-1} \text{ g}^{-1} \text{ biomass}$. The units for ethanol and acids production rates are $\text{mmol hr}^{-1} \text{ g}^{-1} \text{ biomass}$. (a) Growth rate = 0.1 hr^{-1} , formate production = 0. (b) Growth rate = 0.2 hr^{-1} , formate production = 0. (c) Growth rate = 0.1 hr^{-1} , formate production was assumed to equal the sum of the ethanol and acetate production rates; (d) Growth rate = 0.2 hr^{-1} , formate production was assumed to equal the sum of the ethanol and acetate production rates.

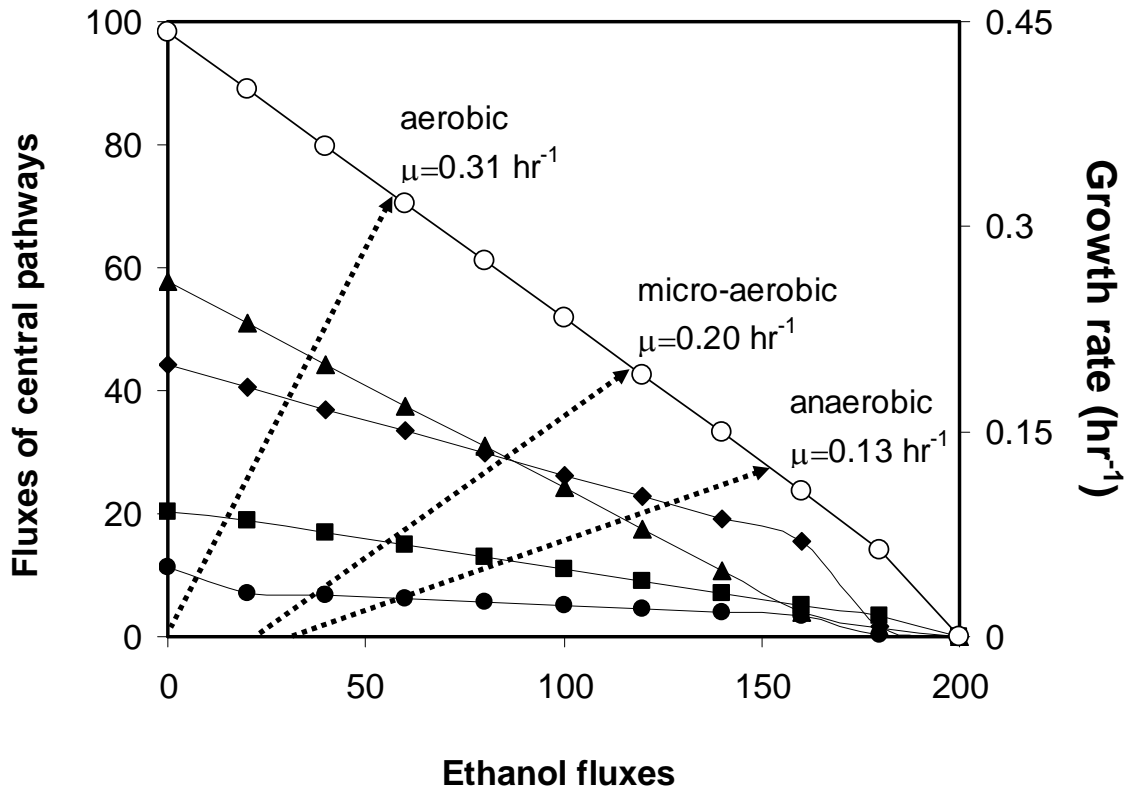


Figure 5. Change in central metabolism as a function of ethanol production as predicted by the *in silico* flux balance model (Simpheny). The objective function used for the calculations was the maximal biomass production. Symbols: growth rate (○); flux into the TCA cycle via citrate synthase (▲); flux into the pentose phosphate pathway via glucose 6-phosphate dehydrogenase (◆) and via transaldolase (GAP+S7P→E4P+F6P) (●); flux through the pyruvate shunt (■). The three dashed arrows **linked** the measured ethanol flux values with their corresponding measured growth rates for the three growth conditions (aerobic, micro-aerobic, and anaerobic). The fact that the dashed arrows **were** not vertical indicated a difference between *in silico* model predicted fluxes (optimal metabolism) and experimentally measured fluxes (actual metabolism).

Tables

Table 1. Enzyme activities in cell extracts of *Geobacillus thermoglucosidasius* M10EXG under three oxygen conditions (n=3).

Enzymes	EC number	Specific activity (units g protein ⁻¹)		
		Aerobic	Micro-aerobic	Anaerobic
Oxalacetate decarboxylase (- Na ⁺)	EC 4.1.1.3	0	3 ± 3	0
Oxalacetate decarboxylase (+ Na ⁺)	EC 4.1.1.3	0	2 ± 3	0
Malic Enzyme (NADP+)	EC 1.1.1.40	0	0	0
Malic Enzyme (NAD+)	EC 1.1.1.38	0	0	0
α-ketoglutarate dehydrogenase	EC 1.2.4.2	230 ± 52	92 ± 75	26 ± 18
Pyruvate carboxylase	EC 6.4.1.1	682 ± 385	660 ± 279	615 ± 246
PEP carboxykinase	EC 4.1.1.49	249 ± 50	373 ± 25	298 ± 22
Isocitrate lyase	EC 4.1.3.1	26 ± 2	22 ± 4	21 ± 5
PEP carboxylase	EC 4.1.1.31	89 ± 58	79 ± 70	49 ± 21
Transhydrogenase	EC 1.6.1.1.	0	0	0

Note: one unit catalyzes the formation of one μmol of substrate per minute.

Table 2. Growth kinetics and yields of ethanol and organic acids under the three oxygen conditions: aerobic growth (G + O₂), micro-aerobic growth (G + μO₂), anaerobic growth (G - O₂).

Yield ¹	G + O ₂	G + μO ₂	G-O ₂ ²	Max ³
Y _{ace/s}	0.64±0.12	0.40±0.05	0.61±0.10	2.6
Y _{lact/s}	0.02±0.01	0.67±0.07	0.89±0.06	2
Y _{etho/s}	0.01±0.01	0.28±0.04	0.38±0.07	2
Y _{form/s}	0	0.13±0.05	1.03±0.14	5.6
Y _{biomass/s}	0.27±0.05	0.19±0.04	0.08±0.03	0.34
Growth rate, hr ⁻¹	0.31±0.04	0.20±0.04	0.13±0.03	0.44

¹Metabolite yield unit, mol metabolites mol⁻¹ glucose. Biomass yield unit, DCW g⁻¹ glucose.

²A small amount of succinate was also detected.

³The maximum yield for each metabolite was predicted using Simpheny. The model assumed a glucose uptake rate equal to 5 mM hr⁻¹ DCW⁻¹.